Received: 10 January 2022 | Revised: 17 May 2022 | Accepted: 20 May 2022

DOI: 10.1002/gcc.23069

RESEARCH ARTICLE

WILEY

Primary mediastinal large B-cell lymphoma is characterized by large-scale copy-neutral loss of heterozygosity

Stefania Tuveri[1] | Koen Debackere[2,3] | Lukas Marcelis[4,5] | Nicolas Dierckxsens[1] | Jonas Demeulemeester[1,6] | Eftychia Dimitriadou[1] | Daan Dierickx[7] | Pierre Lefesvre[8] | Karen Deraedt[9] | Carlos Graux[10] | Lucienne Michaux[1] | Jan Cools[1,3] | Thomas Tousseyn[4,5] | Joris Robert Vermeesch[1] | Iwona Wlodarska[1]

[1]Center for Human Genetics, KU Leuven, Leuven, Belgium

[2]Laboratory for Experimental Hematology, KU Leuven, Leuven, Belgium

[3]Center for Cancer Biology, VIB, Leuven, Belgium

[4]Translational Cell and Tissue Research, KU Leuven, Leuven, Belgium

[5]Department of Pathology, University Hospitals Leuven, Leuven, Belgium

[6]Cancer Genomics Laboratory, The Francis Crick Institute, London, UK

[7]Department of Hematology, University Hospitals Leuven, Leuven, Belgium

[8]Department of Pathology, Free University Hospital, Brussels, Belgium

[9]Anatomo-Pathology, Hospital East Limburg, Genk, Belgium

[10]Department of Hematology, Mont-Godinne University Hospital, Yvoir, Belgium

Correspondence
Iwona Wlodarska, Center for Human Genetics, Herestraat 49, B-3000 Leuven, Belgium.
Email: iwona.wlodarska@uzleuven.be

Funding information
Fonds Wetenschappelijk Onderzoek, Grant/Award Numbers: FWO12J6921, FWO1S74420N; Kom op tegen Kanker; Stichting Tegen Kanker, Grant/Award Number: 2°14-083; KULeuven, Grant/Award Number: C1/018

Abstract

Development of primary mediastinal B-cell lymphoma (PMBL) is driven by cumulative genomic aberrations. We discovered a unique copy-neutral loss of heterozygosity (CN-LOH) landscape of PMBL which distinguishes this tumor from other B-cell malignancies, including the biologically related diffuse large B-cell lymphoma. Using single nucleotide polymorphism array analysis we identified large-scale CN-LOH lesions in 91% (30/33) of diagnostic PMBLs and both investigated PMBL-derived cell lines. Altogether, the cohort showed 157 extra-large (25.3–248.4 Mb) CN-LOH lesions affecting up to 14 chromosomes per case (mean of 4.4) and resulting in a reduction of heterozygosity an average of 9.9% (range 1.3–51%) of the genome. Predominant involvement of terminal chromosomal segments suggests the implication of B-cell specific crossover events in the pathogenesis of PMBL. Notably, CN-LOH stretches non-randomly clustered on 6p (60%), 15 (37.2%), and 17q (40%), and frequently co-occurred with homozygous mutations in the *MHC I* (6p21), *B2M* (15q15), and *GNA13* (17q23) genes, respectively, as shown by preliminary whole-exome/genome sequencing data. Altogether, our findings implicate CN-LOH as a novel and distinct mutational process contributing to the molecular pathogenesis of PMBL. The aberration acting as "second hit" in the Knudson hypothesis, ranks as the major mechanism converting to homozygosity the PMBL-related driver genes. Screening of the cohort of 199 B cell leukemia/lymphoma whole-genomes revealed significant differences in the CN-LOH landscape of PMBL and other B-cell malignancies, including the biologically related diffuse large B-cell lymphoma.

KEYWORDS
primary mediastinal B-cell lymphoma, CN-LOH, SNPa, driver genes, mutations, whole exom/genome sequencing

Joris Robert Vermeesch and Iwona Wlodarska share senior co-authorship.

1 | INTRODUCTION

Cancer genomes are characterized by instability and a progressive accumulation of genetic aberrations, including DNA mutations and chromosomal alterations targeting proto-oncogenes and/or tumor suppressor genes (TSG).[1] Inactivation of the latter genes is usually achieved by two molecular hits targeting both alleles of TSG, typically by a loss-of-function mutation of one allele and deletion of the wild-type allele, leading to loss of heterozygosity (LOH).[2] Segmental and numerical chromosomal losses are instrumental for LOH, but occasionally, LOH can arise without copy number changes due to uniparental disomy (UPD) [alias copy-neutral LOH (CN-LOH)]. The occurrence of UPD, two chromosomes/segments of the same parental origin caused by meiotic segregation errors, was originally described in constitutional diseases.[3] The estimated prevalence of germline UPD in a general population is 1:2000 birth.[4] More recently, somatically acquired UPD/CN-LOH events have been recurrently detected in cancer.[5] These aberrations contribute to genomic instability of tumors and potentially converts TSG to homozygosity when combined with a precedent loss-of-function mutation of one allele, segmental loss of the wild-type allele, and subsequent compensatory duplication of the mutated allele.[6] Alternatively, CN-LOH lesions play a role in the activation of harbored oncogenes, as shown in polycythemia vera where the gain-of-function V617F mutation of *JAK2* is doubled by UPD9p.[7,8]

Pathogenesis of UPD/CN-LOH is incompletely understood. Both germline (meiotic origin) UPD and somatic (mitotic origin) UPD affect whole chromosomes as well as chromosomal segments. The settings of these genetic abnormalities, however, are different and it remains elusive whether the same mechanisms are involved in their pathogenesis. Whole-chromosome CN-LOH presumably arises by monosomy or trisomy rescue, known to attribute to germine UPD. The former is a chromosome gain generated via the non-disjunction of monosomy, whereas the latter is a chromosome loss resulting from non-disjunction of a supernumerary chromosome.[9] Segmental CN-LOH instead arises from homologous somatic (mitotic) recombination after double-strand breaks (DSB) in DNA enriched in fragile sites of the genome.[10] Due to the lack of copy number change, tumor-related CN-LOH lesions remain undetected by standard cytogenetic approaches. The development of single nucleotide polymorphism arrays (SNPa)[11] and next-generation sequencing,[12] however, led to a systematic mapping of CN-LOH events in a wide variety of solid tumors and hematological neoplasms, including non-Hodgkin lymphoma (NHL).[5,13,14] Whether primary mediastinal B-cell lymphoma (PMBL), an aggressive subtype of NHL, harbors CN-LOH remains unknown. SNPa analysis of two PMBL-derived cell lines, Karpas 1106P and U-2940, followed by molecular allelokaryotyping of 33 cases of primary PMBL uncovered numerous extra-large CN-LOH stretches present in the vast majority of analyzed samples. The landscape of these aberrations postulates an important role of CN-LOH in the pathogenesis of PMBL.

2 | MATERIALS AND METHODS

2.1 | Study material

Thirty-two cases of primary PMBL and one case of non-mediastinal PMBL (NM-PMBL)[15] were collected from the database of Center of Human Genetics, KU Leuven and Department of Pathology, University Hospital of Leuven, Belgium. Pathology and clinical records were reviewed. All cases were documented by either DNA or freshly frozen diagnostic biopsy material. Archival cytogenetic pellets were available in 15 cases. The institutional review board "Commissie Medische Ethiek" of the University Hospital approved this retrospective study and renounced the need for written informed consent (Study number S56035, ML10127: January 31, 2014).

Two PMBL-derived cell lines, Karpas 1106P[16] and U-2940[17] were purchased from ECACC (European Collection of Authenticated Cell Cultures) and ATCC (American Type Culture Collection), respectively.

2.2 | Methods

PMBL samples were investigated by SNP arrays (Illumina HumanCytoSNP-12v2.1 BeadChip), fluorescence *in situ* hybridization (FISH), immunohistochemistry (IHC), whole-exome sequencing (WES) (NovaSeq 6000, Illumina) and whole-genome sequencing (WGS) [NovaSeq 6000 (Illumina), Oxford Nanopore Technology sequencing and a Saphyr Chip G2.3 (Bionano Genomics)]. The applied methods are described in the Appendix S1.

3 | RESULTS

3.1 | PMBL harbors widespread CN-LOH events in addition to copy number alterations

Two PMBL-derived cell lines and 33 cases of primary PMBL were subjected to SNPa analysis. Relevant clinical, pathological and genetic data of the reported cases are shown in Table 1. There were 22 female and 11 male patients with age ranging from 12 to 76 years (mean 34.3). Thirty-two patients showed a bulky anterior mediastinal mass, while involvement of the small intestine (CD23+, CD30+, and MAL+) without involvement of mediastinum was found in one patient (case 28) diagnosed with NM-PMBL.[15] Six patients presented with stage I, 15 with stage II and 11 with stage IV (data not available in case 17).

SNPa analysis of Karpas 1106P and U-2940 detected the previously reported genomic imbalances[18] (Figures S1–S3A) and additionally identified 12 extra-large stretches of CN-LOH in each of the cell line. The involved regions are listed in Table 1 and shown in Figures S1 and S2.

Results of SNPa analysis in 33 patient-derived PMBL specimens, including eight tumor/normal tissue paired samples (Table 1), are summarized in Figures 1A,B and S3. Genomic imbalances (275) were

TABLE 1 Relevant clinical and genetic characteristics

Case no.	Age/ Sex	Tissue	Stage (Ann Arbor)	HLA-DR expression (score)	SNPa findings						
					Relevant CNA		CN-LOH regions				
					Gains	Losses	No	Clonal	Subclonal	Size (bp)	% of the genome
Cell lines											
1	Karpas 1106P			NA	2p16, **9p24**	9p21.3, 15q11.2.21.1, 16p13.13	12	1p13.2p36.32, 1q42.2q44,*3p12.2p25.2*,6q11.1q27, 7q36.1q36.3,8q24.21q24.3,11q13.1q25,15q21.1q26.3, 16q24.1q24.3,17q12q25.3, 19q13.41q13.43,22q12.1q13.33		538537773	17.4
2	U-2940			NA		8q24.21, 9p21.3,16p13.13	12	*2q12.1q22.3*,6p21.1p25.3,*8q13.2q24.21*, 8q24.21q24.3, *9p13.3p21.3*,9p13.3p24.3,14q13.2q32.33, 17q21q25.3,19q13.12q13.43, 20q11.21q13.33,Xq12q21.1,Xq21.33q28		443980691	14.3
Primary PMBL											
3[a]	18/ M	Med	II	NA	9p24		14	6p21.1p25.3, 16p13.11q24.3	1,2q11.2q37.3,3p11.2p26.3,4, 7q31.31q36.3,8,10,11,14,15q11. 1q21.1,17q11.2q26.3,19	1573003707	50.7
4	29/F	Med	I	Neg (0)	2p16, **9p24**	6q22.31q24.3,15	10	1q21.3q44,6p21.32p25.3,10q23.1q26.3,12q21.32q24.33, 13q12.3q34,16q12.1q24,Xp21.1p22.33	8,10p15.3q23.1,11	799870989	25.8
5	40/F	Med	IV	Neg (0)			9	6p12.3p25.3,6q14.1q27,9q21.11q34.3, 17q21.2q25.3	1p11.2p36.33,4,7,16q12.1q24.3,*17p13.1q21.2*	760751472	24.5
6[a]	34/F	Med	II	Neg (0)	2p16		9	3p14.1p26.3,6q22.1q27,17q11.2q25.3	1q21.1q44,6p25.3q15,7q22.1q36.3,9, 13q12.12q34,14	757227604	24.4
7	12/F	Med	I	Pos (3)	9p24		8	5q11.2q35.3,6q15q27,9q13q34.3, 15,16p11.2p13.3,17	3.14	742623280	23.9
8	76/F	Med	IV	NA	**2p16**, 9p24		8	6p21.31p25.3,7p11.21p22.3, 14q24.2q32.33,15q15.2q26.3, 16q12.2q24.3,20q11.21q13.33, Xp22.33q21.31,Xq21.31q28		479482276	15.5
9	35/F	Med	II	Neg (0)	***9p24***		7	6p22.1p25.3,*6q13q23.3*,6q24.1q27,15q11.2q26.3,16q12.1q24.3	2p16.1p25.3, 2p15q37.3	471398345	15.2
10	29/ M	Med	II	NA	9p24		5	1,9q31.1q34.3,16,17q21.2q25.3,19		405841311	13.1
11	45/ M	Med	IV	Neg (1)	2p16, **9p24**		5	6p11.2p25.3,9q13q34.3,11q13.4q25	7p11.2p22.3,13q31.1q34	316452187	10.2
12	32/F	Med	I	Neg (0)	2p16, 9p24		5	7p22.3p12.1, *7q31.31q36.2*,9p21.3q34.3,15q11.1q21.3	*5q14.3q33.1*	284220006	9.2
13	16/F	Med	IV	Neg (0)			4	6p21.32p25.3,11q13.1q25	15q11.2q26.3,Xp22.33q26.3	279687902	9
14	34/ M	Med	I	NA			4	6q15q27,9q13q34.3,15q13.3q26.3,17q21.2q25.3		260668480	8.4
15[a]	14/ M	Med	IV	Pos (3)	2p16		4	6p12.3p25.3,15,16q11.2q24.3	4q32.1q35.2	226261232	7.3
16	45/F	Med	I	Neg (0)	2p16, **9p24**	6q23.2q24.3	3	3q21.3q29,*6p12.3p25.3*,15q15.1q26.3		218469036	7
17	49/ M	Med	NA	NA	2p16, 9p24		3	6	7p11.2p22.3,10q22.3q26.3	217681789	7

(Continues)

TABLE 1 (Continued)

Case no.	Age/Sex	Tissue	Stage (Ann Arbor)	HLA-DR expression (score)	SNPa findings						
					Relevant CNA		CN-LOH regions				
					Gains	Losses	No	Clonal	Subclonal	Size (bp)	% of the genome
18	41/F	Med	IV	Neg (0)	**9p24**		3	6p21.32p25.3,8p12p23.3,X		195177485	6.3
19	43/M	Med	II	Pos (3)	2p16, 9p24	6p21.32p22.1, 6q22.3q24.1, 16p13.13	3	6p22.1p25.3,*6p11.1p21.32*,15q11.2q26.3		179482645	5.8
20	29/F	Med	II	Pos (3)	2p16, **9p24**	6q22.3q24.1	3	6p12.2p25.3,12q13.12q24.33,17q22q25.3		164087668	5.3
21[a]	31/M	Med	II	Neg (0)	**9p24**	15q11.1q21.1	3	11p13.1q25, *16q11.2q23.3*	7p11.2p22.3	163977512	5.3
22[a]	30/M	Med	II	Pos (2)	2p16, 9p24		3	8p21.2p23.3,8q13.1q24.3,*17q11.1q23.2*		163148399	5.3
23	35/F	Med	I	Neg (1)	**9p24**		3	*5q23.1q35.1*,6q15q27	3q13.31q29	144703695	4.7
24[a]	37/F	Med	IV	Pos (3)	9p24		3	6p21.33p25.3,17q22q24.3	7p11.2p22.3	142476810	4.6
25	40/F	Med	IV	Neg (1)	2p16, 9p24		2	6p21.31p25.3,17q21.2q25.3		135110147	4.4
26	20/F	Med	II	Pos (3)	**9p24**		2	17q21.2q25.3	1q21.1q44	126039001	4
27[a]	48/F	Med	II	Neg (1)	9p24		2	6p21.1p25.3,16q12.1q24.3		119540830	3.8
28	25/F	SI	IV	NA	2p16		2	13q11q14.2,17q21.31q25.3		86433766	2.8
29	20/F	Med	II	Pos (2)	9p24		2	6p12.1p25.3	1p13.2p36.33	75814373	2.4
30	37/F	Med	II	Neg (1)	9p24		2	6p21.1p25.3,15		69418223	2.2
31[a]	32/F	Med	IV	Pos (2)	2p16, **9p24**		1	6p21.2p25.3		63328178	2.
32	27/F	Med	II	Pos (3)			1	15q13.3q26.3		55975539	1.8
33	45/F	Med	IV	Neg (0)	2p16, 9p24	15	0			40155556	1.3
34	44/M	Med	II	Neg (0)	9p24		0			0	0
35	41/F	Med	II	Neg (0)		6p21.32p22.1	0			0	0

Note: Bold, copy number gains >3; italic, interstitial CN-LO.

Abbreviations: CNA, copy number aberrations; F, female; M, male; Med, mediastinum; NA, not analyzed; Neg, negative; Pos, positive; SI, small intestine.

[a]Tumor/normal tissue paired samples.

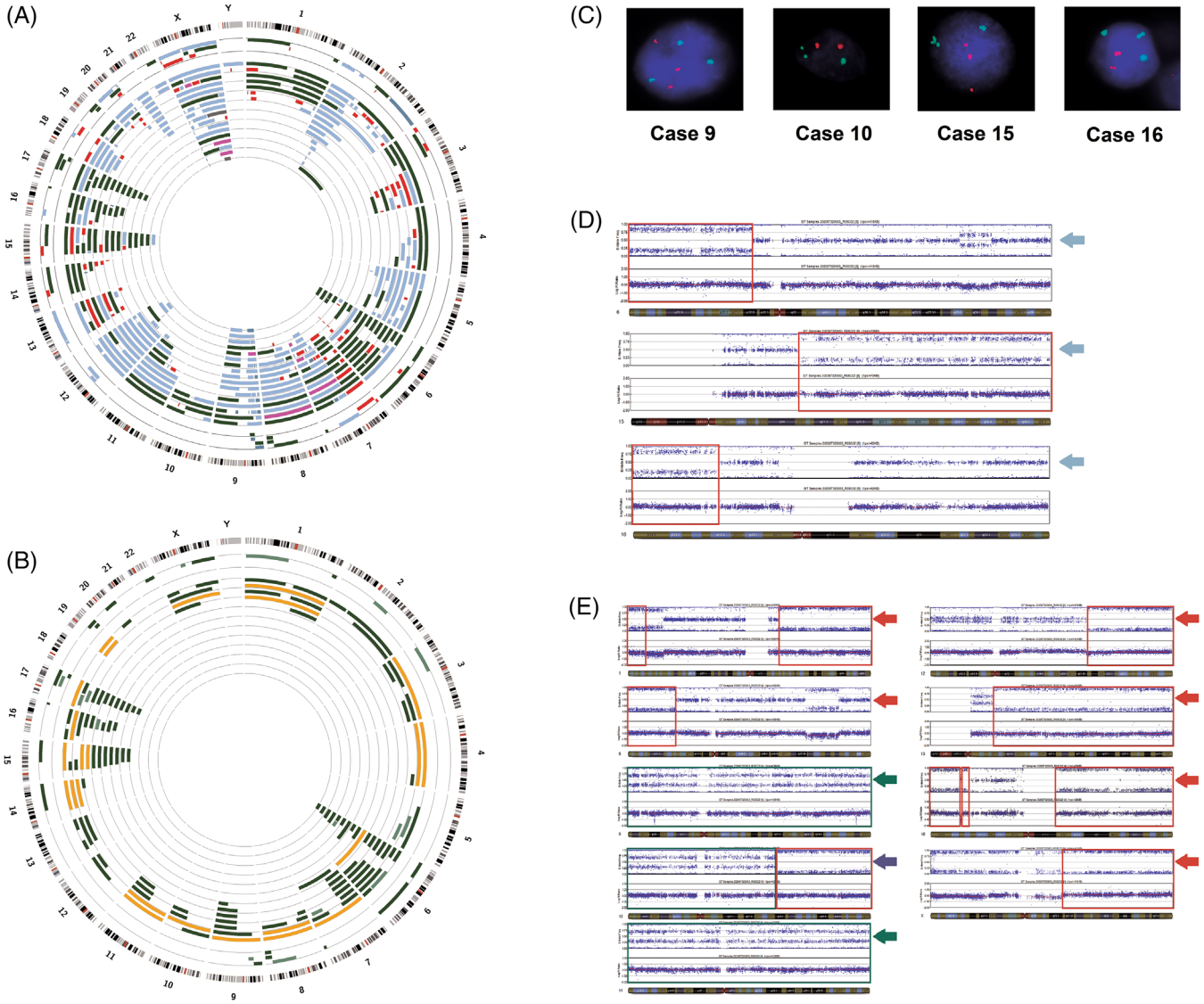

FIGURE 1 Genomic aberrations in PMBL. Circos plots for data visualization. (A) Distribution of all the aberrations detected by SNPa. (B) Distribution of the detected CN-LOH stretches. The two upper layers represent KARPAS-1106P and U2940, while the remaining layers show blocked abnormalities in primary tumors. In (A) red, dark green, light blue, and dark blue tiles mark losses, CN-LOH stretches, gains and gains with >3 copies, respectively. Purple and gray tiles represent AMP-LOH and ambiguous regions (doubts), respectively. In (B) dark green, light green, and orange tiles mark terminal CN-LOH, interstitial CN-LOH, and whole chromosome CN-LOH, respectively. (C) Examples of FISH performed in cases 9 (CEPX-SG/CCND1-SO), 10 (DEK-SG/NUP214-SO), 15 (REL-SO/CEPX-SG), and 16 (IRF4-SO/CEPX-SG). Note two signals of *NUP214* indicative of CN-LOH9q in case 11, two *IRF4* signals confirming CN-LOH6p in case 17, and validation of gain X and 2p16 in cases 9 and 23, respectively. (D–E) Examples of CN-LOH stretches (allele plots) in case 16 and case 4, respectively. In (D) BAF values of 1-0.85-0.15-0 without changes in the LogR value was observed on 6p, 15q, and 16p (light blue arrow). In (E) two recurrent BAF patterns were detected: (I) BAF values of 1-0.92-0.08-0 were found on chr.1p/q, 6p, 10q, 12q, 13q, 16q, and Xp (red arrows) and (ii) BAF values of 1-0.70-0.30-0 were seen on 8, 10p, and 11 (green arrows). Notably, both BAF patterns were observed on chromosome 10 (dark blue arrow). Red and green frames label clonal and subclonal CN-LOH regions, respectively.

detected in all cases (range 2.02–248.45 Mb). Gains were more frequent than losses (207 *vs.* 68; mean 6.2 *vs.* 2.1) and prevalently targeted 9p24 (25/33; 76%), 2p16 (15/33; 45%), 12q (13/33; 39%), Xp (18/33; 55%), Xq (12/33; 38%), 7q (11/33; 34%), 8q (10/33; 30%), 9q (12/33; 36%), 5q (8/33; 24%), 21q (9/33; 27%), 5p (10/33; 30%), and 11q (6/33; 18%). Less numerous genomic losses recurrently involved 6q (7/33; 21%) and 7p (4/33; 12%). In addition to genomic imbalances, SNPa identified 133 segments of somatic CN-LOH (Table 1). To exclude germline CN-LOH lesions potentially representing normal cells present in lymphoma samples, which evidently hampered the early SNPa studies of NHL, we used a stringent threshold of 25 Mb.[19] Lowering the threshold to 10 Mb led to the detection of 39 additional events (Figure S4). Extra-large CN-LOH lesions (>25 Mb) affecting from 1.3% to 51% of the genome (mean 9.5; median 5.79) were detected in 30/33 (91%) diagnostic samples. CN-LOH targeted all chromosomes except 18, 21 and 22 (Figure 1B) and their

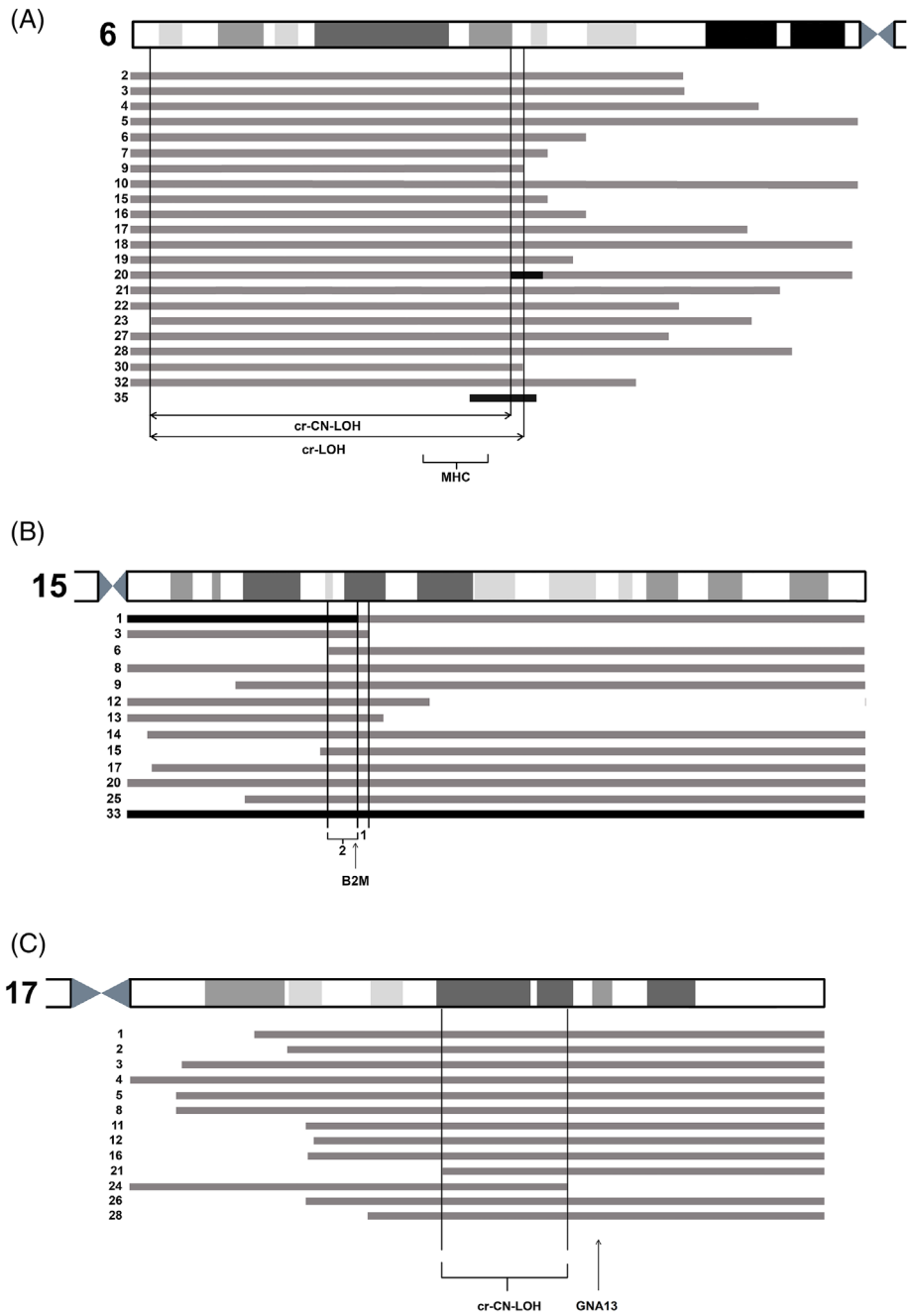

FIGURE 2 The most frequent CN-LOH events in PMBL. (A) CN-LOH6p stretches detected in U-2940 and 20 PMBL cases. (B) CN-LOH15 segments identified in Karpas 1106P and 12 PMBL cases. (C) CN-LOH17q detected in Karpas 1106P, U-2940, and 12 PMBL cases. Ideograms are not in scale. Gray and black bars mark regions of CN-LOH and deletion, respectively. Cases are numbered on the left side of the bars. cr-CN-LOH, common region of CN-LOH; cr-LOH, common region of LOH; 1, indicates cr-CN-LOH; 2 indicates cr-LOH.

frequency ranged from 0 to 14 (mean of 4 and median 3). The CN-LOH defects predominantly affected chromosomal segments (109; 82%) and less frequently whole chromosomes (24; 18%). In the former category, terminal CN-LOH were much more common than interstitial (100 *vs.* 9). The size of segmental CN-LOH stretches ranged from 25.3 to 248.4 Mb (interstitial: 25.3–67.4 Mb; terminal: 26.5–181.2 Mb). None of the extra-large CN-LOH regions identified in primary tumors was present in the eight paired normal controls. Of note, five germline UPDs identified in both tumor and nonmalignant paired samples ranged in size of 0.9–7 Mb.

In six cases with a borderline content of neoplastic cells (<30%), some of the aberrations detected by SNPa were ambiguous (gain *vs.* CN-LOH). To clarify some of them, FISH with probes selected for tested and control (gained or balanced) regions (Table S1) was applied on available cytogenetic specimens. Altogether, we evaluated 11 ambiguous aberrations and validated five regions of CN-LOH and six regions of gain. Gain or normal status of all six control regions were confirmed (Table S2). Representative FISH images are shown in Figure 1C.

Analysis of the average B allele values of particular CN-LOH regions in 28 cases with multiple CN-LOH allowed defining molecular hits underlying generation of CN-LOH in primary tumors. Similar values in multiple CN-LOH regions present in the same sample were found in 11 cases, indicating one hit or clonal selection following the latest CN-LOH event (Figure 1D). Two different values were found in 17 cases (Figure 1E), suggesting the occurrence of two consecutive

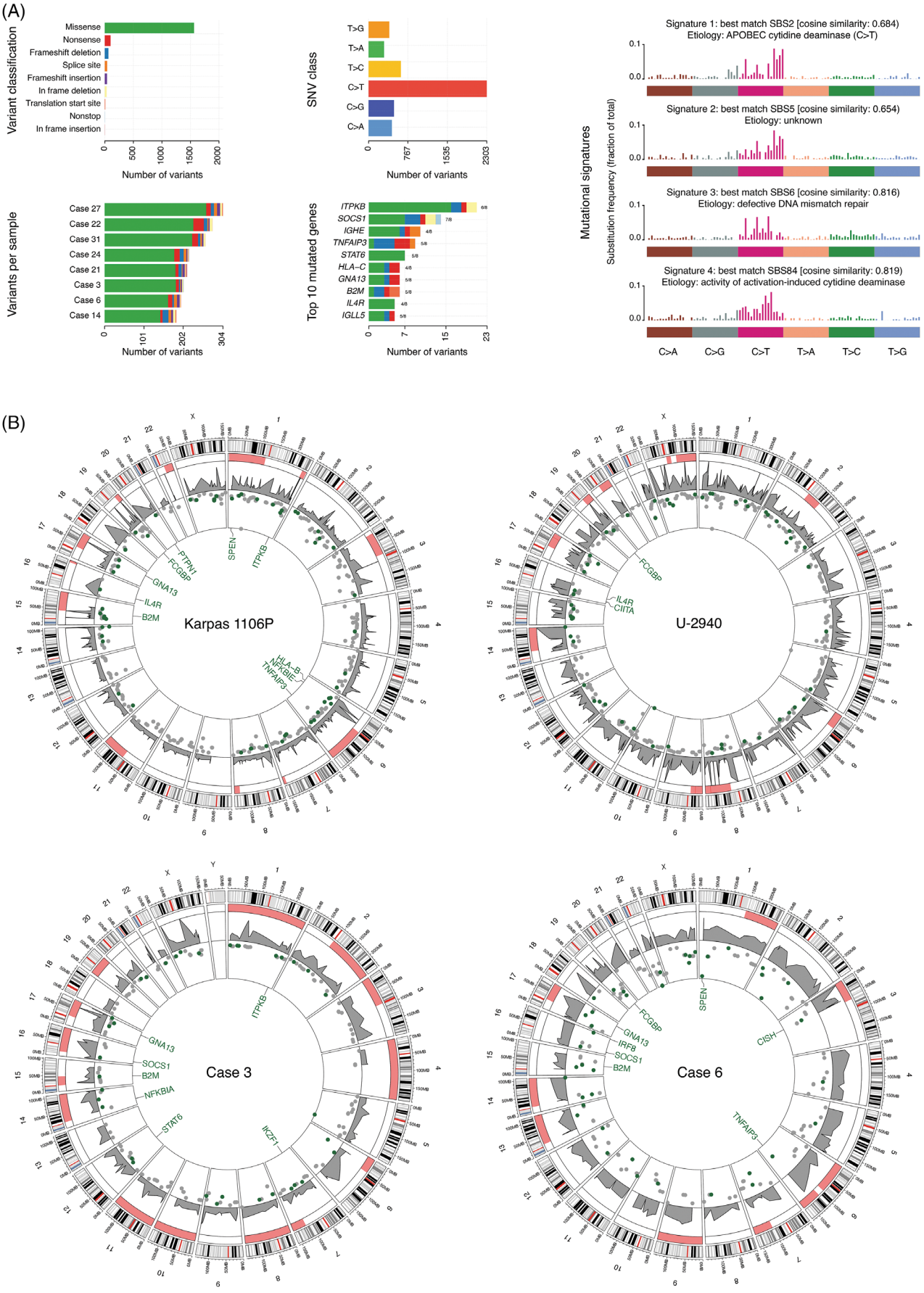

FIGURE 3 Legend on next page.

CN-LOH hits. Consequently, "clonal" and "subclonal" CN-LOH lesions were identified (Table 1). Notably, segmental CN-LOH were preponderantly associated with the first hit (89% *vs*. 65%), while whole-chromosome CN-LOH were more frequent in the second category (35% *vs*. 11%).

CN-LOH stretches were nonrandomly clustered in certain chromosomal regions and affected 6p, 15q, 17q, 1q, 6q, 7p, 14q, 16q, and X in >4 cases. The most prevalent CN-LOH6p was identified in 20 patients and in U-2940 (60%) (Figure 2A). The common region of CN-LOH6p was narrowed down to chr6:1880964-30343703 bp (hg19). CN-LOH15q was detected in 12 patients and in Karpas 1106P (37%) (Figure 2B). The smallest region of CN-LOH was mapped at 15q15.1q21.1 [chr15: 45438537–46702205 bp (hg19)]. CN-LOH17q appeared in 12 patients and in both cell lines (40%) (Figure 2C) and commonly involved 17q22q23.3 [chr17:52759955-62764047 bp (hg19)].

3.2 | Expression of HLA-DR

To determine the expression pattern of the 6p21-related MHC II molecules known to be frequently downregulated in PMBL[20] and their association with CN-LOH6p, 27 cases with available formalin-fixed paraffin-embedded (FFPE) material were subjected to IHC with anti-HLA-DR antigen. Ten cases (37%) (four CN-LOH6p-negative and six CN-LOH6p-positive) expressed HLA-DR, while 17 cases (63%) (six CN-LOH6p-neg and 11 CN-LOH6p-pos) were HLA-DR-negative (Table 1 and Figure S5). The data indicate that CN-LOH is not involved in desregulation of MHC I/HLA-DR.

3.3 | High mutational burden identified by WES/WGS analysis

To characterize the full spectrum of coding sequence mutations in at least part of the studied cases, we subjected eight tumor/normal tissue paired samples (cases 3, 6, 15, 21, 22, 24, 27, and 31) to WES. Altogether, the downstream analysis identified 1851 somatic mutations (mean 231 per tumor-normal pair) involving 237 genes (mean 29.6 per tumor-normal pair) (Table S3). Forty-four genes were affected in >3 cases. Variant classification, single nucleotide variant (SNV) classes, mutational signatures, the number of variants per sample and the top 10 mutated genes are shown in Figure 3A. De novo mutational signature discovery identified 4 signatures. These signatures were compared to COSMIC single base substitution (SBS) signatures v3.0. We identified signatures caused by apolipoprotein B mRNA editing catalytic polypeptide-like (APOBEC) activity, defective DNA mismatch repair and activation-induced cytidine deaminase (AID) activity, congruent with previous studies (Figure 3A).[21,22] *ITPKB*, *SOCS1*, *IGHE*, *TNFAIP3*, *STAT6*, *HLA-C*, *GNA13*, *B2M*, *IL4R*, and *IGLL5* were most frequently affected by SNV and indels, and were found to be mutated in 6, 7, 4, 5, 5, 4, 5, 5, 4, and 5 cases, respectively. All genes, except *IGHE*, *HLA-C*, and *IGLL5*, have been recently recognized as PMBL candidate driver genes.[21,22]

Both cell lines were subjected to WGS. Because of the absence of related normal controls, variant analysis was limited to the coding region of genes with a somatic mutation in at least one of the tumor-normal pairs. We identified 665 mutations involving 120 genes in Karpas 1106P and 642 mutations involving 153 genes in U-2940 (Table S4).

Mutated genes harbored by CN-LOH6p, CN-LOH15q, and CN-LOH17q present in 7, 3, and 6 sequenced cases, respectively, are listed in Table 2. To study the relation between CN-LOH and short variants, we generated Circos plots to visualize the spatial distribution of regions with CN-LOH, variant allele frequency (VAF) and short variants (Figure 3B and Figure S6). Regions of CN-LOH often involved candidate driver genes affected by loss-of-function mutations such as *GNA13*, *B2M*, and *HLA* genes. Candidate driver genes affected by gain-of-function mutations (e.g., *IL4R* or *STAT6*) were never associated with CN-LOH. The VAF of most mutations in regions of CN-LOH was not increased, but notably, the VAF of all *GNA13* mutations, as well as *B2M* and *HLA* genes mutations was compatible with a homozygous mutation.

3.4 | Whole-genome analyses to unravel the CN-LOH mutational signature

We hypothesized that CN-LOH events are driven either by mitotic recombination or by segmental deletions followed by a duplication of the alternative allele. The latter events would result in 2 + 0 copy number states which would resemble the traditional CN-LOH. To determine whether large duplication events do exist and/or to search for mutational scars that could provide a deeper insight into the mechanism(s) underlying the CN-LOH landscape in PMBL, we scanned the genomes of both cell lines by WGS and optical mapping. We produced heatmaps of the percentage of heterozygous variants from the SNP data of Illumina and the detected SVs from Nanopore

FIGURE 3 Integration of CN-LOH and short variant analysis in cell lines and primary PMBL. (A) Results of somatic variant analysis on tumor-normal pairs with a summary of variant classification (top left), a summary of single nucleotide substitutions (top middle), identified mutational signatures and cosine similarity to single base substitution signatures v3 (right), number of variants per sample (bottom left), top 10 genes affected by somatic mutations and the fraction of tumor-normal pairs affected by somatic mutation of the indicated gene (bottom middle). (B) Circos plots for the Karpas 1106P cell line (top left), U-2940 cell line (top right), case 3 (bottom left) and case 6 (bottom right). The outer circle identifies regions of CN-LOH in pink. The middle circle represents the allelic fraction of short variants (SNV and indel) normalized to the variant with the highest allelic fraction. The inner-circle contains a rainfall plot of short variants. Green dots represent variants in genes mutated in more than one tumor-normal pair.

TABLE 2 The most frequent CN-LOH events and co-occurring mutations

	CN-LOH				
Case no	Localization	Start	Stop	Length	Mutated genes
CN-LOH6p					
2	6p21.1p25.3	204909	44469029	44264120	*HIVEP1*, *CDKAL1*, ***H1-3***, *PPP1R3G*
3	6p21.1p25.3	204909	44452157	44247248	***H1-4***, ***H1-3***, *SLC29A1*
6	6p25.3q15	204909	90785351	90580442	*OFCC1*, *MRPL2*, *MCM3*, *ADGRB3*
15	6p12.3p25.3	1880964	50114275	48233311	*FOXC1*, *GCNT2*, ***H3C2***, ***H4C3***,***H1-4***,***HIST1H3D***, ***H3C8***, ***H4C11***, ***H4C12***, ***HLA-C***, ***TNF***, *TAP1*, *DAAM2*
24	6p22.33p25.3	204909	31795550	31590641	*PPP1R3G*,***H1-4***,***H3C7***, ***H2AC11***, ***H1-5***, ***HLA-A***, ***HLA-B***, *LTB*
27	6p21.1p25.3	204909	43213477	43008568	*CDKAL1*, ***TNF***, *BTNL2*, *TBCC*
31	6p21.2p25.3	204909	40360465	40155556	*HIVEP1*, ***H1-2***, *OR10C1*, ***HLA-A***, ***HLA-C***, ***HLA-B***
CN-LOH15q					
1	15q21.1q26.3	45438537	102397836	56959299	*HERC1*, *MYO5C*, *DPP8*, *DUT*
3	15q11.1q21.1	20161372	46702205	26540833	*POTEB3*, *UBE3A*, *TJP1*, *RASGRP1*, *TTBK2*, ***B2M***
15	15q11.1q26.3	20161372	102397836	82236464	***B2M***, *IL16*
CN-LOH17q					
1	17q12q25.3	37357034	81047565	43690531	*CLTC*, *ABCA8*, ***GNA13***, *PRKCA*, *IKZF3*, *KRTAP4-11*, *SMARCE1*
2	17q21q25.3	39884419	69512099	29627680	*CLTC*, *ABCA8*, *NCOR1*, *DNAH9*, *MYH10*, *ACTG1*, *ABCA9*, *PRKCA*, *ARHGAP27*, *CHD3*, *MYH1*, *NOS2*, *SNX11*, *TEX14*, *TMC8*, *UBTF*
3	17q11.2q25.3	31155814	81047565	49891751	*STAT5B*, *ARHGAP27*, *RSAD1*, *CLTC*, *PRR29*, ***GNA13***, *BTBD17*, *RAB37*, *TMC8*, *AATK*
6	17q11.2q25.3	30861865	81047565	50185700	*OR1G1*, *EIF5A*, *DNAH2*, *DNAH9*, *SMARCE1*, ***GNA13***, *H3-3B*
22	17q11.1q23.2	25375921	62764047	37388126	*RHOT1*, *CDK5R1*, *HOXB9*, *TEX14*
24	17q22q25.3	50834441	81041338	30206897	***GNA13***, *ABCA9*, *ACTG1*

Note: Bold, recurrently mutated genes.

(Figure 4A,B) and Bionano (data not shown), each segmented per 7 Mb.[23] The heatmaps of the SNP and SV data resulted in a similar pattern, yet Illumina reads produced the most distinct results as SNP detection with accurate short sequencing reads is more robust than SV calling with long sequencing reads. Overall, those data confirmed the SNP array findings. Notably, no data hinted at the presence of large scale duplication events. To identify possible structural variation scars flanking the CN-LOH regions we analyzed a region of 100 kb flanking the start of those regions. No common CNVs or recurrent scars could be identified. These results suggest the rearrangements are recombination events.

3.5 | Distinctive features of the PMBL-related CN-LOH landscape

To compare the CN-LOH landscape of PMBL with those of other lymphoma entities, we analyzed the previously published WGS data on 199 cases of B-cell malignancies included in the Pan-Cancer Analysis of Whole Genomes (PCAWG)[24] Consortium of the International Cancer Genome Consortium and The Cancer Genome Atlas.[25] The cohort contains 51 cases of DLBCL and 36, 17, and 95 cases of follicular lymphoma (FL), Burkitt lymphoma (BL) and chronic lymphocytic leukemia (CLL), respectively. Like in the SNPa analysis, genomic streches showing a major allele of 2 and a minor allele of 0 were classified as regions of CN-LOH (see Appendix S1). Only events of ≥25 Mb were scored. Altogether, the frequencies of extra-large CN-LOH regions ranged from 80% (DLBCL) to 8.4% (CLL) and the mean/median ranged from 1.8/2 (DLBCL) to 0.09/0 (CLL) (Table 3 and Figure 4C). Differences in frequency of CN-LOH between PMBL and the remaining entities are statistically significant ($p < 0.05$).

4 | DISCUSSION

PMBL is a rare subtype of DLBCL recognized as a separate entity by the recent WHO classification of tumors of hematopoietic and lymphoid tissue.[26] The tumor arises in the mediastinum and predominantly affects young women. The molecular pathogenesis of PMBL is complex and incompletely understood, but the involvement of at least three important pathways, NF-kB, JAK/STAT, and programmed cell death protein 1 (PDL1)-mediated immune evasion, has been recently demonstrated.[21,22] Early and recent studies showed that members of these pathways are frequently targeted by either genomic imbalances

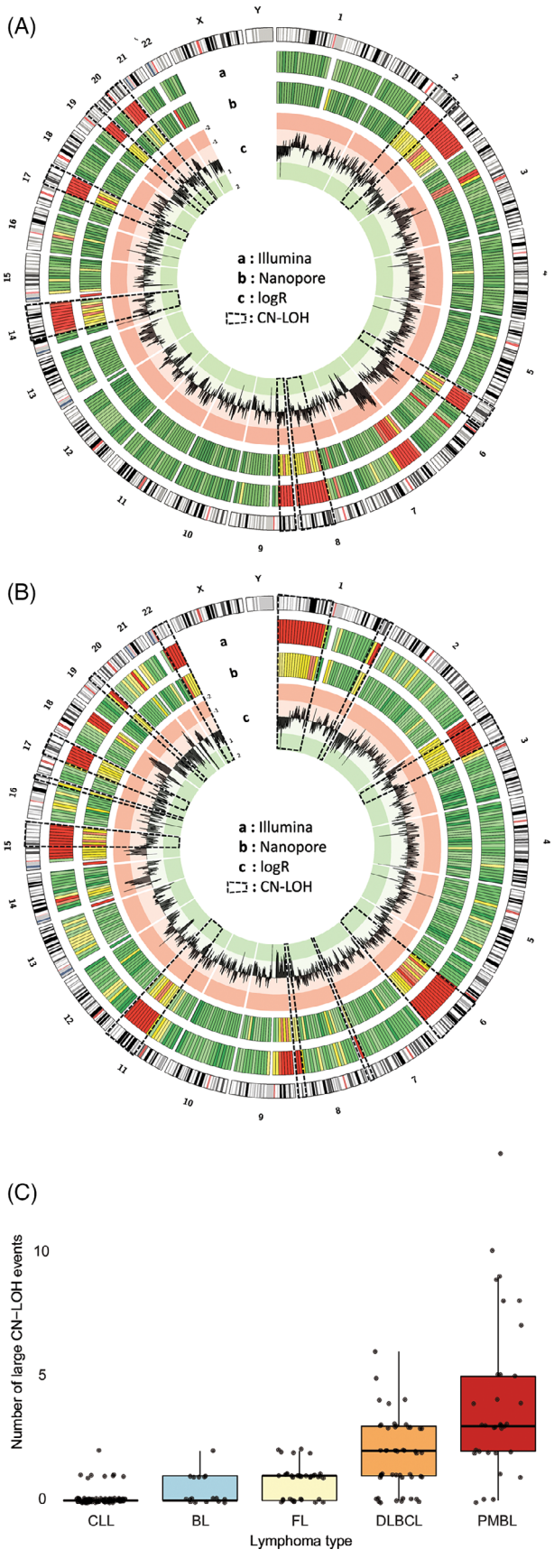

and/or somatic mutations.[21,22,27–29] The most relevant copy number gains affect 9p24.3 (*JAK2-CD274-PDCD1LG2*) (71%) and 2p16.1 (*REL*) (42%).[22] Recurrent mutations have been detected in up to 50 candidate driver genes, including *SOCS1*, *GNA13*, *STAT6*, *ITPKB*, *ACTB*, *TNFAIP3*, *IL4R*, *ZNF217*, *NFKBIE*, *CIITA*, and *IRF2BP2*, that are mutated in 20–60% of cases. Given that each investigated case showed a median of 9 driver mutations[21] and so far, an initial deterministic event was not identified, neoplastic transformation of PMBL seems to be a multistep process triggered by the cumulative somatic aberrations acquired during its evolutionary past.

Our study showed for the first time that PMBL is characterized by large-scale CN-LOH. The lesions differ substantially from CN-LOH events in other tumors, being detected in more than 90% of cases, targeting extra-large genomic segments on multiple chromosomes and reducing heterozygosity of up to 51% (mean 9.9) of the tumor genome. The distinct CN-LOH landscape in PMBL was evidenced by the screening of whole-genomes of 199 B-NHL cases included in the PCAWG cohort[25] (Table 2 and Figure 4C) and revision of the previously published SNPa data.[30–33] None of so far analyzed B-cell malignancies, including a biologically related DLBL and classical Hodgkin lymphoma (cHL),[34] showed a similar landscape of CN-LOH as PMBL The importance of CN-LOH in PMBL is emphasized by recurrence and high incidence of CN-LOH6p (60%), CN-LOH15 (37%), and CN-LOH17q (40%). Notably, these lesions frequently co-occurred with mutations in the *MHC I* genes (*HLA-A/-B/-C*) (43%) and histone/linker histone genes (71%), mutations in *B2M* (67%) and *GNA13* (67%), respectively, as shown by our preliminary integrative analysis (Table 2). MHC (I and II) molecules play an important role in host immunoreaction to tumors, antigens presentation and immune responses.[35] Their perturbed expression in lymphomas, including PMBL,[36,37] is considered a major mechanism of escape from immunosurveillance of cancer cells. As shown previously, defective expression of MHC I in PMBL is mainly driven by loss-of-function alterations of *B2M* (beta-2-microglobulin),[21,22] the gene essential for forming functional MHC I, found to be affected by CN-LOH15. Although CN-LOH6p also covers the MHC II locus, the expression pattern of the HLA-DR protein indicates that the lesion is not involved in the downregulation of this molecule. The mutated histone

FIGURE 4 CN-LOH events across PMBL and other B-cell malignancies. Relative densities of heterozygous variation detected with Illumina and Nanopore WGS data of Karpas 1106P (A) and U2940 (B). The Illumina density plots (a) are derived from 78 229 218 positions and the nanopore plots (b) from consensus SV calls (>50 bp) by combiSV. The logR plots (c) are derived from the coverage of the Illumina dataset. Reduced heterozygous ratios are colored in yellow or red. CN-LOH events are enclosed by dashed lines. (C) Box and scatter plot showing the number of large-scale CN-LOH events detected in samples of the indicated lymphoma type. Each dot represents a single sample. Center line, median; box limits, upper and lower quartiles; whiskers, 1.5× interquartile range.

TABLE 3 Differences in CN-LOH lesions between PMBL and four B-cell lymphoma/leukemia entities

NHL entity	No of analyzed cases	No (%) of cases with CN-LOH	CN-LOH events					References
			Total no	Range	Mean	Median	*p* value	
PMBL	33	30 (91)	133	0–14	4.03	3	0	This study
DLBCL	51	41 (80.4)	92	0–6	1.8	2	0.000028*	[24,25]
FL	36	24 (66.7)	29	0–2	0.8	1	<0.00001*	[24,25]
BL	17	6 (35.3)	7	0–2	0.41	0	<0.00001*	[24,25]
CLL	95	8 (8.4)	9	0–2	0.09	0	<0.00001*	[24,25]
Levels of significance: $^*p < 0.05$								

Abbreviations: BL, Burkitt lymphoma; CLL, chronic lymphocytic leukemia; DLBCL, diffuse large B-cell lymphoma; FL, follicular lymphoma; PMBL, primary mediastinal B-cell lymphoma.

and linker histone genes located at 6p likely perturb interaction of the histones with chromatin and related effector molecules, resulting in an aberrant exposition of DNA to ongoing AID activity and high mutations rate.[38] The *GNA13* (G Protein Subunit Alpha 13) gene codes for Gα13, a component of the Gα12/Gα13 coupled receptor involved in the GPCR signaling. The gene, known to act as a tumor suppressor in B-NHL,[39,40] is preferentially affected by CN-LOH17q in PMBL. Noteworthy, *GNA13* mutations were detected in 6/10 cases analyzed by WES/WGS, including 4/6 tumors (67%) with CN-LOH17q (Table 2). In these four cases, the VAF of all *GNA13* mutations was compatible with a homozygous mutation, providing evidence that the mutation occurred before CN-LOH. In this case, CN-LOH would act as a second hit to inactivate the other allele. Similar observations were made for loss-of-function mutations in *B2M* and *HLA* genes. Together, these data support the hypothesis that CN-LOH lesions act as a second hit to inactivate tumor suppressor genes. This function of CN-LOH could explain significantly less frequent genomic losses in PMBL (25% vs. >50% in DLBCL[41,42] and cHL[43]). Interestingly, the VAF suggests that CN-LOH occurs early in the disease course and that most mutations (except *GNA13*, *B2M*, and *HLA* genes) are acquired after CN-LOH.

The mechanism(s) underlying the generation of CN-LOH in PMBL remains elusive. The prevalent occurrence of segmental CN-LOH in a heterozygous diploid context as well as lack of common CNVs and/or recurrent scars in regions flanking CN-LOH regions point to a key role of mitotic homologous recombination (HR). This mechanism usually follows DSB and likely acts as an errant DNA repair mechanism leading to CN-LOH.[5,44] HR requires close contact of homologous chromosomes, similar to the first meiotic division. The recombined sister chromatids segregate into two daughter cells without a reductional division and subsequent clonal selection results in the expansion of one of the haplotypes (Figure S7). Given that "clonal" (predominantly segmental) CN-LOH are more frequent than "subclonal" (predominantly whole-chromosome) lesions (68% *vs*. 32%), our data suggest that mitotic HR is particularly active during the early stages of lymphomagenesis and the associated hit(s) follows mutagenesis of driver genes but precedes the remaining mutations and genomic imbalances.

Recent integrative genomic studies of PMBL[22] identified several previously uncharacterized mutational processes operating in this tumor, among others a microsatellite instability (MI) signature and AID/APOBEC mutational signature (confirmed by our study). The former is associated with defective DNA mismatch repair and MI, while the activity of latter enzymes is correlated with the occurrence of DSB and DSB repair pathways generating single-stranded DNA stretches, similar to HR. In physiological conditions, AID plays a central role in somatic hypermutation (SHM) and class-switch recombination (CSR) of the immunoglobulin genes in activated B-cells promoting the generation of transient DNA DSB.[45,46] Aberrant AID expression underlies tumorigenesis, contributing to genomic instability and initiating oncogenic events, like CSR-related chromosomal translocations driving B-cell lymphomagenesis.[47] Notably, CN-LOH events affect numerous genes with AID motifs and the top five genes are located on 6p (Table S5). A high level of AID is typically observed in centroblasts of the germinal center but it has also been detected in interfollicular large B-cells and thymic B-cells residing in the thymic medulla.[48] Notably, thymic B-cells displaying a highly activated phenotype are postulated normal counterparts of PMBL.[49] High AID expression possibly exposes B-cells to a sustained accumulation of genetic aberrations in accessible target sequences.[50] Interestingly, PMBL constitutively expresses AID although neoplastic cells are IG-negative, shows a low frequency of CSR and lack of ongoing SHM.[51] Whether the large-scale CN-LOH events identified in PMBL could be attributed to the enhanced activity of the AID/APOBEC pathway or other repair pathways operating in B-cell, like the ubiquitous Base Excision Repair (BER) pathway,[52] needs further investigations. Specific association of large-scale CN-LOH and PMBL might suggest a key role of the mediastinal environment in the induction of these genetic events. The finding of a similar CN-LOH/gain pattern in the case of NM-PMBL (no 28), however, contradicts this supposition.

In conclusion, we show that PMBL is characterized by a landscape of CN-LOH. The aberrations significantly contribute to genetic instability of PMBL converting to homozygosity up to 51% of the genome and potentially misbalancing the expression of thousands of the involved genes, including mutated (Table S6) and imprinted genes (Table S7). Non-random clustering of CN-LOH events points to the

important role of these cytogenetically cryptic aberrations in deregulation of PMBL-associated driver genes and ranks CN-LOH6p as one of the most frequent genetic defects in PMBL, following mutations in *SOCS1* and gain 9p24.[21,22] The mechanism(s) underlying CN-LOH are largely unknown but the involvement of a hitherto undescribed mitotic recombinational driver is postulated. The novel genetic hallmark of PMBL highlights the molecular complexity of the tumor and supports its distinction from the related lymphomas.

ACKNOWLEDGMENT

The authors thank Kathleen Doms, Kim Rummens, and Anne Renmans for their excellent technical assistance.

FUNDING INFORMATION

Research Foundation-Flanders (FWO 1S74420N; FWO 12J6921N), KULeuven (C1/018), Kom op tegen Kanker, Stichting tegen Kanker (2°14-083).

CONFLICT OF INTEREST

The authors declare no conflict of interest.

DATA AVAILABILITY STATEMENT

SNPa, WGS and WES data are deposited in GEO (https://https.ncbi.nlm.nih.gov/geo/query/acc.cgi?acc=GSE184212), ENA (https://www.ebi.ac.uk/ena/browser/view/PRJEB50976) and EGA (EGAS00001006235), respectively.

ORCID

Stefania Tuveri https://orcid.org/0000-0003-4051-4295
Koen Debackere https://orcid.org/0000-0002-7701-326X
Lukas Marcelis https://orcid.org/0000-0002-5446-1801
Nicolas Dierckxsens https://orcid.org/0000-0001-8051-6602
Jonas Demeulemeester https://orcid.org/0000-0002-2660-2478
Eftychia Dimitriadou https://orcid.org/0000-0003-2845-0057
Daan Dierickx https://orcid.org/0000-0002-8917-022X
Carlos Graux https://orcid.org/0000-0001-9236-3623
Joris Robert Vermeesch https://orcid.org/0000-0002-3071-1191
Iwona Wlodarska https://orcid.org/0000-0001-7455-4135

REFERENCES

1. Hanahan D, Weinberg RA. The hallmarks of cancer. *Cell*. 2000;100(1):57-70.
2. Knudson AG. Mutation and cancer: statistical study of retinoblastoma. *Proc Natl Acad Sci USA*. 1971;68(4):820-823.
3. Cassidy SB, Schwartz S. Prader-Willi and Angelman syndromes: disorders of genomic imprinting. *Medicine (Baltimore)*. 1998;77(2):140-151.
4. Nakka P, Pattillo Smith S, O'Donnell-Luria AH, et al. Characterization of prevalence and health consequences of uniparental disomy in four million individuals from the general population. *Am J Hum Genet*. 2019;105(5):921-932.
5. Tuna M, Knuutila S, Mills GB. Uniparental disomy in cancer. *Trends Mol Med*. 2009;15(3):120-128.
6. Maciejewski JP, Mufti GJ. Whole genome scanning as a cytogenetic tool in hematologic malignancies. *Blood*. 2008;112(4):965-974.
7. Kralovics R, Passamonti F, Buser AS, et al. A gain-of-function mutation of JAK2 in myeloproliferative disorders. *N Engl J Med*. 2005;352(17):1779-1790.
8. Levine RL, Wadleigh M, Cools J, et al. Activating mutation in the tyrosine kinase JAK2 in polycythemia vera, essential thrombocythemia, and myeloid metaplasia with myelofibrosis. *Cancer Cell*. 2005;7(4):387-397.
9. O'Keefe C, McDevitt MA, Maciejewski JP. Copy neutral loss of heterozygosity: a novel chromosomal lesion in myeloid malignancies. *Blood*. 2010;115(14):2731-2739.
10. Young BD, Debernardi S, Lillington DM, et al. A role for mitotic recombination in leukemogenesis. *Adv Enzyme Regul*. 2006;46(1):90-97.
11. Mao X, Young BD, Yong-Jie L. The application of single nucleotide polymorphism microarrays in cancer research. *Curr Genomics*. 2007;8(4):219-228.
12. Nielsen R, Paul JS, Albrechtsen A, Song YS. Genotype and SNP calling from next-generation sequencing data. *Nat Rev Genet*. 2011;12(6):443-451.
13. Etebari M, Navari M, Piccaluga PP. SNPs array karyotyping in non-Hodgkin lymphoma. *Microarrays*. 2015;4(4):551-569.
14. Song J, Shao H. SNP array in hematopoietic neoplasms: a review. *Microarrays*. 2015;5(1):1.
15. Yuan J, Wright G, Rosenwald A, et al. Identification of primary mediastinal large B-cell lymphoma at nonmediastinal sites by gene expression profiling. *Am J Surg Pathol*. 2015;39(10):1322-1330.
16. Nacheva E, Dyer MJS, Metivier C, et al. B-cell non-Hodgkin's lymphoma cell line (Karpas 1106) with complex translocation involving 18q21.3 but lacking BCL2 rearrangement and expression. *Blood*. 1994;84(10):3422-3428.
17. Sambade C, Berglund M, Lagercrantz S, et al. U-2940, a human B-cell line derived from a diffuse large cell lymphoma sequential to Hodgkin lymphoma. *Int J Cancer*. 2006;118(3):555-563.
18. Dai H, Ehrentraut S, Nagel S, et al. Genomic landscape of primary mediastinal B-cell lymphoma cell lines. *PLoS One*. 2015;10(11):e0139663.
19. Tiu RV, Gondek LP, O'Keefe CL, et al. New lesions detected by single nucleotide polymorphism array-based chromosomal analysis have important clinical impact in acute myeloid leukemia. *J Clin Oncol*. 2009;27(31):5219-5226.
20. Roberts RA, Wright G, Rosenwald AR, et al. Loss of major histocompatibility class II gene and protein expression in primary mediastinal large B-cell lymphoma is highly coordinated and related to poor patient survival. *Blood*. 2006;108(1):311-318.
21. Chapuy B, Stewart C, Dunford AJ, et al. Genomic analyses of PMBL reveal new drivers and mechanisms of sensitivity to PD-1 blockade. *Blood*. 2019;134(26):2369-2382.
22. Mottok A, Hung SS, Chavez EA, et al. Integrative genomic analysis identifies key pathogenic mechanisms in primary mediastinal large B-cell lymphoma. *Blood*. 2019;134(10):802-813.
23. Dierckxsens N, Li T, Vermeesch JR, et al. A benchmark of structural variation detection by long reads through a realistic simulated model. *Genome Biol*. 2021;22(1):342.
24. Campbell PJ, Getz G, Korbel JO, et al. Pan-cancer analysis of whole genomes. *Nature*. 2020;578(7793):82-93.
25. Gerstung M, Jolly C, Leshchiner I, et al. The evolutionary history of 2658 cancers. *Nature*. 2020;578(7793):122-128. doi:10.1038/s41586-019-1907-7
26. Swerdlow SH, Campo E, Pileri SA, et al. The 2016 revision of the World Health Organization classification of lymphoid neoplasms. *Blood*. 2016;127(20):2375-2390.
27. Joos S, Otaño-Joos MI, Ziegler S, et al. Primary mediastinal (thymic) B-cell lymphoma is characterized by gains of chromosomal material including 9p and amplification of the REL gene. *Blood*. 1996;87(4):1571-1578.
28. Wessendorf S, Barth TFE, Viardot A, et al. Further delineation of chromosomal consensus regions in primary mediastinal B-cell

lymphomas: an analysis of 37 tumor samples using high-resolution genomic profiling (array-CGH). *Leukemia*. 2007;21(12):2463-2469.
29. Green MR, Monti S, Rodig SJ, et al. Integrative analysis reveals selective 9p24.1 amplification, increased PD-1 ligand expression, and further induction via JAK2 in nodular sclerosing Hodgkin lymphoma and primary mediastinal large B-cell lymphoma. *Blood*. 2010;116(17):3268-3277.
30. Pfeifer D, Pantic M, Skatulla I, et al. Genome-wide analysis of DNA copy number changes and LOH in CLL using high-density SNP arrays. *Blood*. 2007;109(3):1202-1210.
31. Scholtysik R, Kreuz M, Klapper W, et al. Detection of genomic aberrations in molecularly defined Burkitt's lymphoma by array-based, high resolution, single nucleotide polymorphism analysis. *Haematologica*. 2010;95(12):2047-2055.
32. Cheung KJJ, Delaney A, Ben-Neriah S, et al. High resolution analysis of follicular lymphoma genomes reveals somatic recurrent sites of copy-neutral loss of heterozygosity and copy number alterations that target single genes. *Genes Chromosom Cancer*. 2010;49(8):669-681.
33. Sebastián E, Alcoceba M, Martín-García D, et al. High-resolution copy number analysis of paired normal-tumor samples from diffuse large B cell lymphoma. *Ann Hematol*. 2016;95(2):253-262.
34. Otto C, Giefing M, Massow A, et al. Genetic lesions of the TRAF3 and MAP3K14 genes in classical Hodgkin lymphoma. *Br J Haematol*. 2012;157(6):702-708.
35. Kelly A, Trowsdale J. Genetics of antigen processing and presentation. *Immunogenetics*. 2019;71(3):161-170.
36. Riemersma SA, Jordanova ES, Schop RFJ, et al. Extensive genetic alterations of the HLA region, including homozygous deletions of HLA class II genes in B-cell lymphomas arising in immune-privileged sites. *Blood*. 2000;96(10):3569-3577.
37. Rimsza LM, Roberts RA, Miller TP, et al. Loss of MHC class II gene and protein expression in diffuse large B-cell lymphoma is related to decreased tumor immunosurveillance and poor patient survival regardless of other prognostic factors: a follow-up study from the leukemia and lymphoma molecular. *Blood*. 2004;103(11):4251-4258.
38. Chapuy B, Stewart C, Dunford AJ, et al. Molecular subtypes of diffuse large B cell lymphoma are associated with distinct pathogenic mechanisms and outcomes. *Nat Med*. 2018;24(5):679-690.
39. Muppidi JR, Schmitz R, Green JA, et al. Loss of signalling via G α 13 in germinal centre B-cell-derived lymphoma. *Nature*. 2014;516(7530):254-258.
40. O'Hayre M, Inoue A, Kufareva I, et al. Inactivating mutations in GNA13 and RHOA in Burkitt's lymphoma and diffuse large B-cell lymphoma: a tumor suppressor function for the Gα13/RhoA axis in B cells. *Oncogene*. 2016;35(29):3771-3780.
41. Lenz G, Wright GW, Emre NCT, et al. Molecular subtypes of diffuse large B-cell lymphoma arise by distinct genetic pathways. *Proc Natl Acad Sci U S A*. 2008;105(36):13520-13525.
42. Scholtysik R, Kreuz M, Hummel M, et al. Characterization of genomic imbalances in diffuse large B-cell lymphoma by detailed SNP-chip analysis. *Int J Cancer*. 2015;136(5):1033-1042.
43. Wienand K, Chapuy B, Stewart C, et al. Genomic analyses of flow-sorted Hodgkin Reed-Sternberg cells reveal complementary mechanisms of immune evasion. *Blood Adv*. 2019;3(23):4065-4080.
44. Makishima H, Maciejewski JP. Pathogenesis and consequences of uniparental disomy in cancer. *Clin Cancer Res*. 2011;17(12):3913-3923.
45. Muramatsu M, Sankaranand VS, Anant S, et al. Specific expression of activation-induced cytidine deaminase (AID), a novel member of the RNA-editing deaminase family in germinal center B cells. *J Biol Chem*. 1999;274(26):18470-18476.
46. Muramatsu M, Kinoshita K, Fagarasan S, Yamada S, Shinkai Y, Honjo T. Class switch recombination and hypermutation require activation-induced cytidine deaminase (AID), a potential RNA editing enzyme. *Cell*. 2000;102(5):553-563.
47. Ramiro AR, Jankovic M, Eisenreich T, et al. AID is required for c-myc/IgH chromosome translocations in vivo. *Cell*. 2004;118(4):431-438.
48. Moldenhauer G, Popov SW, Wotschke B, et al. AID expression identifies interfollicular large B cells as putative precursors of mature B-cell malignancies. *Blood*. 2006;107(6):2470-2473.
49. Perera J, Huang H. The development and function of thymic B cells. *Cell Mol Life Sci*. 2015;72(14):2657-2663.
50. Pettersen HS, Galashevskaya A, Doseth B, et al. AID expression in B-cell lymphomas causes accumulation of genomic uracil and a distinct AID mutational signature. *DNA Repair (Amst)*. 2015;25:60-71.
51. Popov SW, Moldenhauer G, Wotschke B, et al. Target sequence accessibility limits activation-induced cytidine deaminase activity in primary mediastinal B-cell lymphoma. *Cancer Res*. 2007;67(14):6555-6564.
52. Stratigopoulou M, van Dam TP, Guikema JEJ. Base excision repair in the immune system: small DNA lesions with big consequences. *Front Immunol*. 2020;11:1084.

SUPPORTING INFORMATION

Additional supporting information may be found in the online version of the article at the publisher's website.

How to cite this article: Tuveri S, Debackere K, Marcelis L, et al. Primary mediastinal large B-cell lymphoma is characterized by large-scale copy-neutral loss of heterozygosity. *Genes Chromosomes Cancer*. 2022;61(10):603-615. doi:10.1002/gcc.23069